Phys. Status Solidi C **7**, No. 7–8, 1749–1755 (2010) / **DOI** 10.1002/pssc.200983444

physica status solidi c
www.pss-c.com
current topics in solid state physics

The nucleation of HCl and Cl_2-based HVPE GaN on mis-oriented sapphire substrates

Tim Bohnen[1], Gerbe W. G. van Dreumel[1], Jan L. Weyher[2], Willem J. P. van Enckevort[1], Hina Ashraf[1], Aryan E. F. de Jong[1], Paul R. Hageman[*,1], and Elias Vlieg[1]

[1] IMM, Radboud University, Heyendaalseweg 135, 6525 AJ Nijmegen, The Netherlands
[2] Institute of High Pressure Physics, Polish Academy of Sciences, ul. Sokolowska 29/37, 01-142 Warsaw, Poland

Received 29 September 2009, revised 19 January 2010, accepted 27 January 2010
Published online 18 May 2010

Keywords GaN, VPE, nucleation, morphology, structure, annealing

[*] Corresponding author: e-mail P.Hageman@science.ru.nl, Phone: +31-24-3653158, Fax: +31-24-3652314

The nucleation of both classic HCl-based and novel Cl_2-based HVPE GaN on mis-oriented sapphire substrates was investigated. The use of Cl_2 in HVPE increases the growth rate by a factor of 4-5 and strongly reduces the parasitic deposition, allowing for the growth of much thicker wafers than HCl-based HVPE. Morphological SEM surface studies of the HCl-based HVPE sample surface show that at 600 °C a nanocrystalline layer is deposited on the sapphire. During the subsequent annealing phase, the morphology changes to a µm-sized island structure. During overgrowth at 1080 °C, the islands coalesce. Small voids or pinholes are then formed in between the coalescing GaN islands. These pinholes lead to numerous pits on the surface of the GaN at thicknesses of 5 µm. The pits disappear during continued overgrowth and can no longer be found on the surface, when the GaN film reaches a thickness of 45 µm. This particular coalescence mechanism also applies to Cl_2-based HVPE GaN on sapphire.

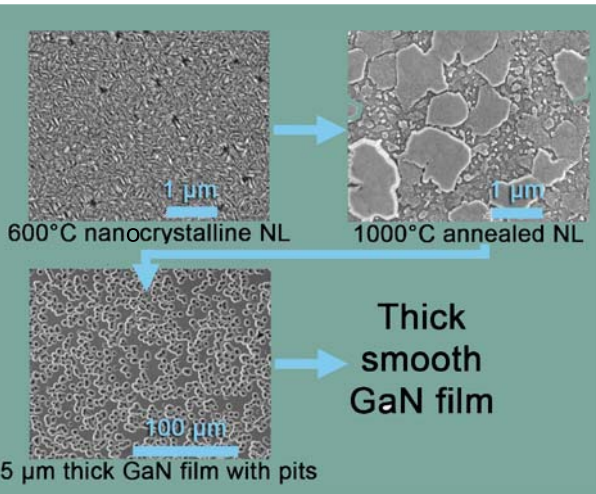

The different stages of HVPE GaN on sapphire: a 600 °C nanocrystalline nucleation layer, which is annealed at 1080 °C into an island structure. These islands in turn coalesce during overgrowth, resulting in the formation of numerous pits, which will eventually disappear after continued overgrowth.

1 Introduction The performance of GaN-based devices is often limited by defects acting as electron-hole pair recombination centers or as scattering centers that limit thermal conductivity. In typical GaN devices one comes across a multitude of structural defects, such as dislocations and inclusions of cubic GaN. Another common defect is the so-called pinhole, which is often found in large numbers in the first micrometer of the GaN layer [1–3]. These V-shaped defects consist of a void with an inverted pyramidal shape [4] and can introduce screw dislocations [4] or result in the formation of nanopipes in the crystal layers [2,5]. The pinhole defect in this work is not to be confused with the inverted pyramids or V-pits, which are often observed on the surface of > 100 µm thick HVPE GaN layers [6,7].

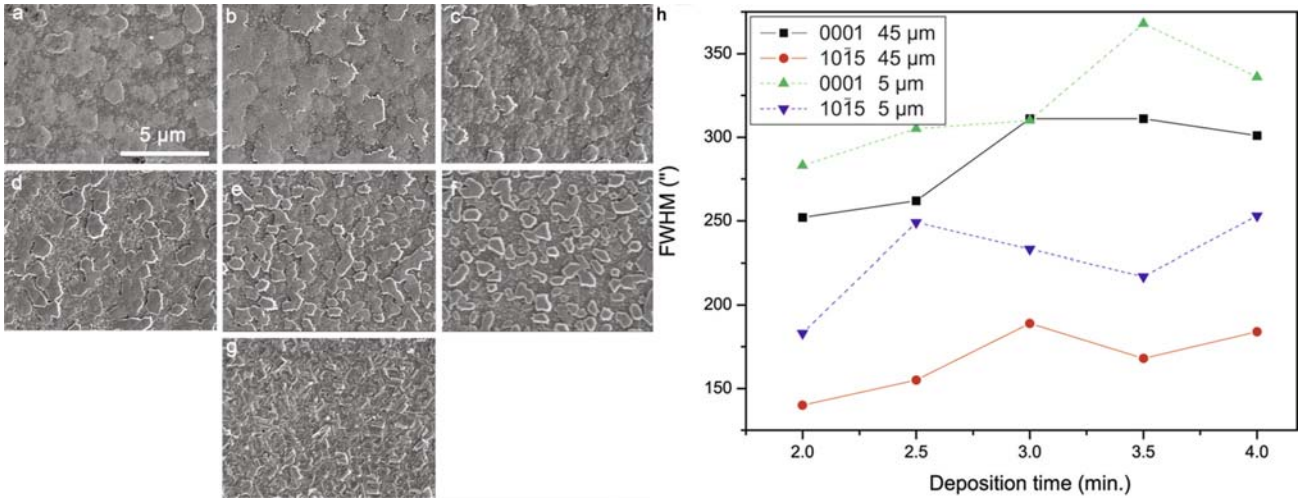

Figure 1 The morphology of the annealed nucleation layers with a fixed GaCl flow and an increasing deposition time of 1, (a), 2 (b), 2.5 (c), 3 (d), 3.5 (e), 4 (f), and 15 (g) minutes. The full width half maxima (FWHM) of the HRXRD rocking curves measurements for the symmetric 0 0 0 1 and asymmetric 1 0 $\bar{1}$ 5 peaks are plotted as a function of the deposition time between 2 and 4 minutes for the annealed nucleation layers, overgrown with 5 and 45 µm of HVPE GaN (h).

Commonly, a buffer or nucleation layer is applied to the sapphire substrate to overcome the mismatch between GaN and sapphire [8]. The preparation of such a GaN nucleation layer has been extensively studied for MOCVD, but not for HVPE. The transitions in the morphology of the low temperature GaN nucleation layer, as it is prepared for thin film overgrowth by annealing in an ammonia atmosphere after deposition, has been well researched by Koleske *et al.* for MOCVD GaN [9, 10]. In contrast, little is known about the nucleation of HVPE GaN (see for example [11]).

The substitution of HCl by Cl_2 in HVPE results in a $5\times$ increase in growth rate (400 µm/h vs. 80 µm/h for equally large flows) and a strong reduction in parasitic deposition, enabling the growth of 1.2 mm thick GaN films in a single growth run, in contrast to 300 µm by HCl-based HVPE. Using Cl_2 doubles the molar density of Cl atoms. It also alters the formation reaction of GaCl by eliminating H-containing byproducts, that are formed when using HCl and can block the Ga surface from the Cl precursor. Also the change in standard enthalpy GaCl formation reaction is slightly more negative for Cl_2 and Cl_2 molecules are more weakly bound than HCl. Additionally, the increased flow of GaCl to the GaN surface facilitates a faster removal of Cl from the growing GaN face in accordance with the model by Cadoret *et al.* [12](submitted to *J. Cryst. Growth* and was presented at the IWBNS-6). In view of these findings, we also investigated the nucleation of GaN on bare sapphire to grow GaN films using Cl_2-based HVPE.

In this paper we investigate the nucleation of HCl-based HVPE GaN on mis-oriented sapphire substrates. We will show that the nucleation of GaN by Cl_2-based HVPE on such sapphire substrates is possible and that the nucleation proceeds in a similar manner for both HCl-based and Cl_2-based HVPE.

2 Experimental section

2.1 HCl-based HVPE The HCl-based HVPE GaN films were grown in a horizontal 4 inch home-built HVPE reactor on small pieces cut from 2 inch (0 0 0 1) sapphire wafers with a miscut of 0.3° towards the *a* lattice direction [13]. This mis-orientation of the substrate was used to enforce a step flow growth mode. Scholz *et al.* have shown this improves the crystal quality and smoothness of epitaxial GaN layers [14].

First, the sapphire substrates were heated to 1000 °C at 200 mbar, cleaned in H_2-containing atmosphere for 3 minutes, and then nitridated for 10 minutes under a constant NH_3 flow. Subsequently, the samples were cooled to approximately 600 °C at which point NH_3 was combined with GaCl obtained from the direct reaction between liquid Ga and gaseous HCl to form the GaN nucleation layer. The deposition times in this nucleation step were 1, 2, 2.5, 3, 3.5, 4, and 15 minutes for the different experiments with a fixed gallium precursor flow of HCl flow of 30 sccm HCl to ensure similar supersaturations.

Next, the samples were heated to the growth temperature of 1080°C under a constant NH_3 flow in approximately half an hour and then slowly cooled to room temperature. This high temperature NH_3 annealing of the nanocrystalline nucleation layers (Fig. 3) changes their morphologies to those seen in Fig. 1, a process thoroughly studied for MOCVD GaN by Koleske *et al.* [9]. As the heating of our HVPE reactor is slow ($\sim\frac{1}{2}$ hour), the nucleation layer will have reached a stable state during this phase. We found no significant changes in crystal quality of the thick GaN layers when the nucleation layers were annealed, cooled to room temperature, and reheated to be overgrown in a single growth run as compared to

nucleation layers, that were directly overgrown after the annealing phase.

Finally, the samples were cut and, for each nucleation layer deposition time, a piece was placed in the reactor for overgrowth by the combination of NH_3 and GaCl. The other pieces were used to investigate the morphology of the annealed nucleation layers. A 5 and a 45 μm thick GaN layer were deposited on the nucleation layers at 1080°C and at a pressure of 950 mbar using hydrogen as the main carrier gas. These thicknesses were chosen in order to study the overgrowth in its initial and final stages. For each overgrowth time, all pieces with the different nucleation deposition times were placed together in the reactor to ensure identical overgrowth conditions for all the samples.

2.2 Cl_2-based HVPE A similar experiment was performed in a home-built 2 inch Cl_2-based HVPE reactor. Here, the deposition time was fixed to 3 minutes while the Cl_2 flow during nucleation as varied between 17, 19, 22, and 25 sccm. In this case the nucleation layers were overgrown with an approximately 30 μm and 0.7 mm thick Cl_2-based HVPE GaN film in separate growth experiments.

The annealed nucleation layers and overgrown samples were characterized by optical microscopy, (cross-sectional) scanning electron microscopy (SEM), optical interferometry, $\theta/2\theta$ X-ray diffraction (XRD) measurements, and rocking curve HRXRD scans. Defect selective etching was performed in a molten eutectic of KOH/NaOH above400 °C for an appropriate time to reveal all dislocations [15]. Photoetching was performed in a stirred aqueous KOH solution utilizing the UV light from a Xe lamp [16].

3 Results

3.1 Nucleation of classical HCl-based HVPE GaN Figure 3 shows the morphology of typical nucleation layer after 3 minutes of deposition at 600 °C. The average size of the crystallites is in the nano-range and does not exceed 250 nm. Most crystallites appear elongated in a preferential direction; the overall texture appears to possess a six-fold symmetry. When the sample is subsequently heated under a constant NH_3 flow to the growth temperature of 1080 $°C$, the morphology of the nucleation layer changes into an μm-sized island structure, as can be seen in Figs. 1a to g. The height of the islands on a single sample varies between 20 and 200 nm, as was determined by interferometry, for deposition times between 2 and 4 minutes (Figs. 1b to f). The nucleation layers in Figs. 1a and g, which were grown with deposition times of 1 and 15 minutes, did not result in single-crystalline thin GaN films after overgrowth.

No major changes can be seen in the morphology of nucleation layers after high temperature annealing, as the thickness of the low temperature nucleation layer is increased (Fig. 1a-g). $\theta/2\theta$ XRD measurements confirmed that all out-of-plane orientations of the annealed nucleation layers were similar. The sidefaces of the islands in Figs. 1a through e appear to broaden with increasing deposition time, suggesting an increase in the island height as the deposition time is increased. Lateral expansion, on the other hand, appears to have been significantly smaller. The exception being Fig. 1g, which was grown with a lengthy deposition time of 15 minutes: The GaN nuclei have begun overlapping one another.

The preferential direction of the island edges formed via the step flow growth mode enforced by the misorientation can still be distinguished in Figs. 1a and b, but it is no longer visible in Figs. 1c to g. In Figs. 1a and b the edges of the individual islands are very curved and ragged, disturbing the step flow direction. This ragging effect appears to decrease for increasing island height, as can be seen in Figs. 1a through g.

Finally, the overgrown nucleation layers were examined. Only the nucleation layers with deposition times between 2 and 4 minutes yielded smooth transparent GaN layers. The sample that was overgrown with a deposition time of 1 minute resulted in an incomplete surface coverage of GaN on top of the nucleation layer. The 15 minute sample led to the formation of polycrystalline GaN atop the nucleation layer. The characterization was therefore focused on the samples which yielded a smooth thin film of GaN.

The structural quality of the GaN layers was probed by XRD and defect-selective etching. After cutting, pieces of the 45 μm thick overgrown samples were etched in a KOH/NaOH eutectic, which selectively attacks defects. Dislocation densities were counted and all lie between 1 and 2×10^8 cm^{-2} with the majority of the dislocations being of mixed or edge type. This was confirmed by rocking curve XRD measurements, where the full width half maxima of the peaks are related to the dislocation densities [17, 18], as can be seen in Fig. 1h. The structural quality of the GaN layer increases with increasing thickness. The full width half maxima of both the symmetric 0 0 0 1 and asymmetric 1 0 $\bar{1}$ 5 peaks decrease as the layer thickness is increased from 5 to 45 μm (Fig. 1h). Admittedly not very clearly, but a slight increase in the full width half maxima of the HRXRD peaks as the nucleation layer's deposition time is increased can be seen in Fig. 1h. Shorter deposition times during nucleation reduce the XRD peak width but below 2 minutes of deposition the nucleation layer becomes too thin, resulting in incomplete surface coverage and polycrystalline GaN growth after continued overgrowth.

Oddly, the 5 μm thick high temperature GaN layer present on top of the nucleation layers is not completely coalesced (Figs. 2e and k). Numerous pits of different sizes are found on the surface in Fig. 2k. These pits are filled as the thickness increases and the 45 μm thick GaN layer in Fig. 2l shows no such pits (Figs. 2l).

To understand the transition from nucleation layer into a GaN thin film, a cross-sectional SEM study was performed. An annealed nucleation layer, grown with a deposition time of 4 minutes, is shown in Fig. 4g. Figure 4h

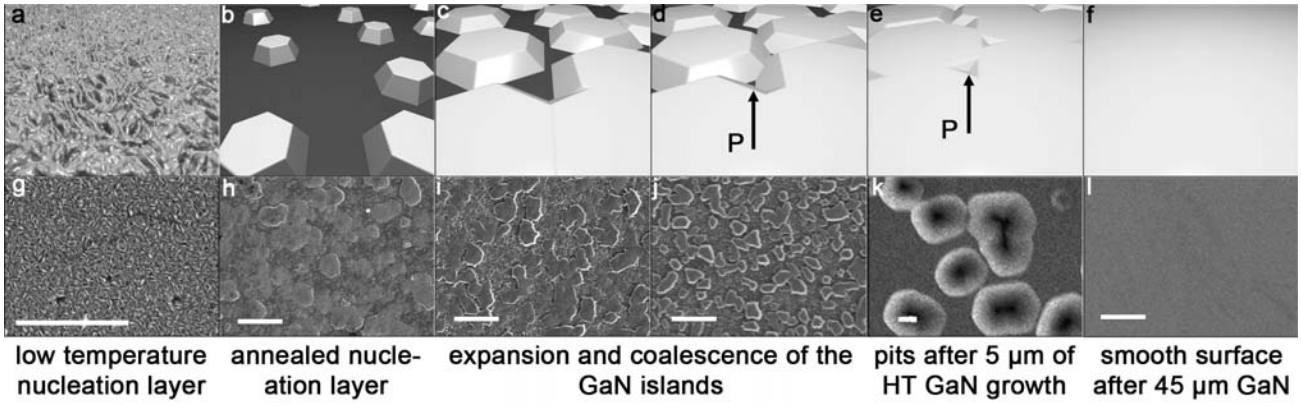

Figure 2 Schematic representation (a-f) and SEM images (g-l) of the surface morphology of the GaN during the various stages of the HVPE nucleation-annealing-overgrowth process. Bar is 1 µm.

depicts the cross-section of a 45 µm thick GaN on sapphire sample after etching in molten KOH/NaOH, whereas Fig. 4i shows the cross-section after photo-etching. All cross-sections were obtained by cleaving the 45 µm thick GaN on sapphire samples after the growth.

We find columnar structures originating at the sapphire surface, when examining the cross-section of an eutectically etched sample. These columns join one another in a continuous layer, roughly 1 µm above the surface of the sapphire substrate (Fig. 4h). As the eutectic etches dislocations faster than defect-free GaN, the empty spaces between the columns must have contained highly defective material prior to the etching, in contrast to the columns themselves, which consist of high quality GaN.

Photo-etching was applied to better understand the structure of the high temperature GaN layer. The cross-sections of all samples were subjected to photo-etching, which is known to reveal both dislocations and electrically active defects, as was demonstrated by Weyher *et al.* and Lewandowska *et al.* [16, 19]. The etch rate during photo-etching is inversely proportional to the carrier concentration [16]. In all samples triangular-shaped volumes showing numerous small hillocks or pits, which are separated by V-shaped structures, marked '(a)' in Fig. 4i, were revealed along the interface.

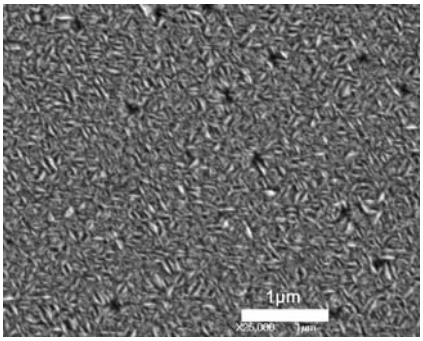

Figure 3 SEM image of the unannealed nanocrystalline low temperature GaN nucleation layer, grown with 3 minutes deposition time.

The V-shaped structures themselves consist of two different zones: a slowly etched V-shaped zone, marked '(a)' in Fig. 4i, and a central zone with clear growth striations, labeled '(b)'. Following the inversely proportional relationship between the etch rate (etch depth) and the carrier concentration established by Lewandowska *et al.* [16], the V-shaped zone '(a)' has a higher carrier concentration than the surrounding matrix, most probably because of the non-$\langle 0\ 0\ 0\ 1 \rangle$ growth directions indicated by the tilted black arrow in Fig. 4i. Though the exact mechanism for this change in carrier concentration is not fully understood, Lewandowska *et al.* suggested that more impurities were incorporated on the non-Ga-faces in these other growth directions [16]. These growth directions are different from the middle of the striation at site '(b)', as indicated by the black arrow, pointing upward in the $\langle 0\ 0\ 0\ 1 \rangle$ direction. As the V-shaped regions, marked '(a)', were hardly etched, these regions appear smooth.

The areas in between the V-shapes were also etched very slowly, but large concentrations of dislocations gave rise to the numerous pits or hillocks that appear as black spots in these regions. The carrier concentration in the regions, labeled '(b)' in Fig. 4i, is low compared to that of the V-shaped regions, marked '(a)' and the etching resulted in the clear growth striations, which are an indication of the high crystal quality of the material in the central region '(b)'.

3.2 Nucleation of Cl_2-based HVPE The nucleation of Cl_2-based HVPE proceeds similar to that of classical HCl-based HVPE. The morphologies of the Cl_2-based HVPE nucleation layers in Fig. 5b and c show a similar island structure as those in Fig. 1a to f. The nucleation layers in Figs. 5a and d appear to be more coalesced than Figs. 5b and c.

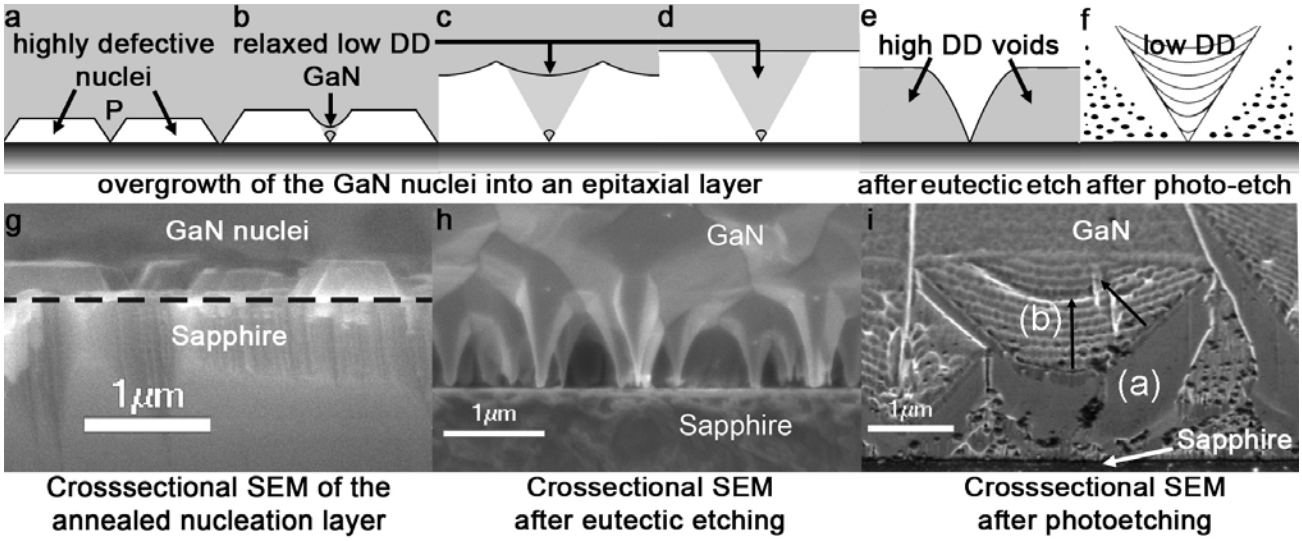

Figure 4 Schematic model of the pinhole formation in HVPE GaN during the coalescence of the GaN nuclei (a-f) and cross-sectional SEM images of the annealed GaN 4 minutes deposition time nucleation layer, showing the GaN nuclei on the sapphire (g), the GaN-sapphire interface after etching in molten KOH/NaOH (h), and the GaN-sapphire interface after photo-etching (i).

Overgrowth of a 30 μm thick GaN layer on the nucleation layers of Figs. 5a and d will yield a thin GaN film but the majority of the surface is covered by numerous small pits, with the exception of the wafer's edges. Continued overgrowth into a 0.7 mm thick layer results in the formation of polycrystalline GaN on top of the nucleation layers of Figs. 5a and d. The nucleation layers in Figs. 5b and c, however, yield smooth thin GaN films even at thicknesses of 0.7 mm.

After the deposition of 30 μm of GaN on the nucleation layers, all 4 samples still posses a single-crystalline thin GaN film. This was determined by the single peak found after HRXRD, as shown in Fig. 6. The full width half maxima are comparable to those of the HCl-based HVPE layers, suggesting a dislocation density in the order of 10^8 cm^{-2} for the nucleation layers, shown in Figs. 5b and c.

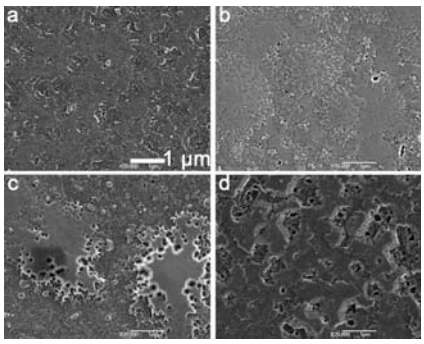

Figure 5 SEM images of the annealed nucleation layers, deposited in 3 minutes with a Cl_2 flow of 17 (a), 19 (b), 22 (c), and 25 sccm (d).

Similar pits as those that were observed for HCl-based thin GaN layers in Fig. 2b, are found on the surface of the 30 μm thick GaN films. The density of pits is significantly higher on the samples yielding polycrystalline GaN after continued overgrowth of 0.7 mm of GaN. The pit density on these samples clearly increases when moving from the wafer edges (which yield smooth GaN films upon continued overgrowth) towards the center (which after overgrowth becomes polycrystalline). Near the center the pit density becomes too high to distinguish individual pits and hillocks are formed, which, in turn, are covered by small pits.

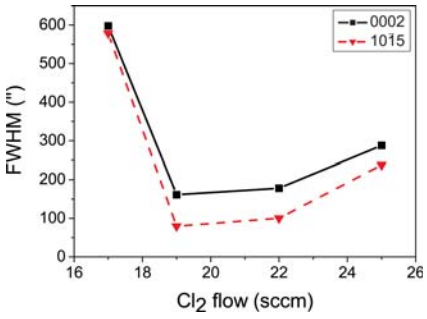

Figure 6 Full width half maxima of the peaks of the rocking curve HRXRD measurements on the 30 μm thick GaN films, grown on the nucleation layers in Fig. 5, versus the supplied Cl_2 flow.

Figure 6 depicts the dislocation densities of the 30 μm thick GaN layers, overgrown on the nucleation layers of Fig. 5. Using 17 and 25 sccm of Cl_2 during the 3 minutes

of nucleation results in layers, which will yield polycrystalline material upon further overgrowth of 0.7 mm of GaN (Figs. 5a and d). These GaN layers are not smooth and reflective, but opaque due to the presence of numerous pits. Also, the 0 0 0 2 HRXRD peak widths for these sample are high, ∼600". However, the nucleation layers, prepared with Cl_2 flows of 19 and 21 sccm, will maintain their single crystalline thin film appearance upon further overgrowth. Their dislocation densities are much lower, but increase with increasing Cl_2 flow during nucleation. A similar trend was observed for HCl-based nucleation layers in Fig. 1h.

4 Discussion

4.1 Nucleation of classical HVPE GaN The annealing phase drastically alters the morphology of the nucleation layer. The initial low temperature nucleation layer changes from its nanocrystalline structure in Fig. 3 to the islands-dominated morphologies in Fig. 1a to g during annealing. According to Koleske *et al.*, this is due to the decomposition of GaN, which starts roughly above $800^{\circ}C$ (activation energy is 2.7 eV), and recrystallization in the presence of NH_3 [9]. The morphology of the annealed HVPE nucleation layers is different from MOCVD [9], but the mechanisms, proposed by Koleske *et al.* for MOCVD, can in all likelihood be applied here for HVPE. The growth rate in HVPE is higher than in MOCVD, which most likely resulted in an increased deposition of GaN during nucleation. Also, the heating ramp in HVPE is significantly slower.

The increase in island size and decrease in island density during annealing suggest some form of Ostwald-ripening to minimize the surface energy (see e.g. Kim *et al.* [20]). Smaller islands are decomposed to be partially incorporated into larger ones. The decomposition of GaN above 800 °C aids this process. Combined with the diffusion of particles over the surface, this further enhances the growth of the larger islands through ripening and smoothening effects. Additionally, the slower temperature ramp in HVPE compared to MOCVD will enhance any of the above mentioned effects.

Though different deposition times were applied, the nucleation layers after annealing in Figs. 1a to f appear similar for all deposition times below 4 minutes. The average island size and density appear constant with increasing deposition time. The islands' edges, however, become more pronounced and straight as the sidefaces attempt to minimize their surface free energy, thereby removing the ragging effect, caused by defect pinning of the expanding sidefaces [21]. The fact that the sidefaces become wider with increasing deposition times, suggests an increase in island height, assuming the crystallographic orientation of the sidefaces is the same for all islands in Figs. 1a to f. Figure 1g shows that, given a sufficiently long deposition time, the growth mode of the nucleation layer changes to yield overlapping and stacked nuclei, which, in turn, results in a polycrystalline layer after overgrowth.

The entire process of HVPE nucleation and overgrowth is outlined Figs. 2 and 4. The transition of the nucleation layer during annealing is discussed above. In the subsequent phase the annealed nucleation layer is overgrown, starting with the coalescence of the individual GaN islands (Figs. 2b-d). Unlike MOCVD [9], the overgrown GaN layer has not fully coalesced after 5 µm, as can be seen from the numerous pits in the GaN surface in Figs. 2e and k. These pits are eventually filled as the layer thickness is increased.

The origin of the pits is outlined in the coalescence and overgrowth model, described schematically in Figs. 2 and 4. As the annealed nucleation layer is overgrown, nuclei start to expand in specific crystallographic directions, determined by the shape of the annealed GaN islands. The growth rate of the top (0 0 0 1) plane is the largest, which leads to the formation of roughly pyramidal structures. Due to the GaN-sapphire mismatch the structural quality of these GaN pyramids will be poor, resulting in a high dislocation density in these areas.

The pits are formed during the coalescence of the GaN nuclei. During expansion, nuclei will encounter one another in the lateral direction forming low angle grain boundaries (see Figs. 2d and 4a). Eventually, the whole surface will be GaN-covered, with the exception of small vacant areas in between the GaN nuclei, indicated by 'P' in Figs. 2d and e. The large GaN-sapphire mismatch has induced a large mis-orientation in the GaN nuclei with respect to one another. The strain on the GaN in points such as indicated by 'P' in Fig. 2e will be therefore be large. This, combined with the steep inclination of the sidefaces of the nuclei, leads to the formation of a small void. The large strain at this point is eliminated by including such a pinhole defect in the GaN layer. The vacant area 'P' is overgrown from the sidefaces of the nuclei (Fig. 4b). The void or pinhole allows the GaN that is grown above it to relax, reducing the number of defects (Fig. 4c).

This explains the striations seen after photo-etching. These striations, marked '(b)' in Fig. 4i, posses a good structural quality compared to the triangular regions, dotted with dark spots, in between the V-shaped structures, labeled '(a)' (compare Figs. 4d, f and i). The striations were grown above the small voids or pinholes, while the spotted poor quality triangles corresponded to the sites of the GaN nuclei (Fig. 4b, c, and d). The smooth V-shaped structures in Fig. 4h indicate the transitional region between the highly defective GaN from the nuclei and the relaxed high quality material above the pinhole (Figs. 4f and i), where growth took place exclusively on the sidefaces of the GaN nuclei (Fig. 4b). This change in growth direction accounts for the differences in carrier concentration, as indicated by the etch depth in Fig. 4i [16, 19].

Similarly, we can explain the columns that are found after orthodox etching in Fig. 4h. These columns posses a higher quality GaN than the material that was etched away, since the etch rate for etching in molten eutectic in-

creases with increasing the dislocation density. The bottoms of the columns indicate the sites of the pinholes, while the columns themselves correspond with the locations of the striations above the pinholes (Figs. 4d, e, and h). The highly defective GaN, grown on the nuclei, was etched away while the columnar regions of relaxed and high quality GaN persist. Alternatively, the rapid orthodox etching can be related to the sideways bending of threading dislocations during the 3 dimensional expansion of the GaN nuclei, as discussed by Zhao *et al.* [22]. Etching proceeds fastest in the direction of the dislocation.

4.2 Nucleation of Cl_2-based HVPE The Cl_2-based HVPE nucleation layers also posses an island structure (Fig. 5). While the nucleation layers in Figs. 5b and c are suited for thin film epitaxy, the nucleation layers in Figs. 5a and d result in incomplete surface coverage or overlapping GaN islands, respectively. In both cases, polycrystalline GaN is produced upon overgrowth.

Despite similar island structures, the actual GaN islands grown by Cl_2-based HVPE, are different from those grown by HCl-based HVPE. This, in all likelihood, are related to the higher growth rates of the Cl_2-based method. Especially in Fig. 5b, the islands are more rounded and the edges are more ragged. As stated above, the ragging is caused by defect pinning of the expanding sidefaces. The deep trenches in Fig. 5b suggest a locally decreased mobility of the steps on the expanding sidefaces [23].

The pit formation mechanism described for HCl-based HVPE can be clearly seen during coalescence of the Cl_2-based GaN nuclei (Fig. 5). When comparing Fig. 5b to c, we can distinguish the pit formation during the coalescence of the individual islands, as shown schematically in Fig. 2. In Fig. 5c, the larger islands with the hexagonal shapes have expanded in the lateral direction with respect to the islands in Fig. 5b. When the expanding sidefaces encounter other islands, pits are formed. Figure 5c clearly shows how the pits remain on the islands' top surfaces as the edges of the island grow further and further outward. The sidefaces of the pits appear to be very stable and possess low growth rates, which accounts for the fact that the pits are still visible after continued overgrowth of 30 µm of GaN.

5 Conclusions We studied the nucleation of HCl-based and Cl_2-based HVPE GaN. At 600 °C a nanocrystalline GaN layer is deposited, which, most likely by a decomposition and recrystallization process during the annealing under NH_3 to the growth temperature of 1080 °C, is changed into separate, µm-sized flat islands. During the overgrowth phase, these islands coalesce and, at the meeting points between expanding nuclei, pinholes are formed, due to the high strain on the GaN in the meeting point. The pinholes allow for a local relaxation of the GaN above them, which eventually expands into a continuous high quality GaN layer.

Additionally, we have demonstrated that the nucleation of Cl_2-based HVPE GaN on mis-oriented sapphire substrates is possible and that the nucleation proceeds in a similar manner as in classic HCl-based HVPE.

Acknowledgements The funding of this work by the Dutch Organization for Scientific Research (STW-NWO) is gratefully acknowledged.

References

[1] A. M. Sánchez, P. Ruterana, M. Benamara, and H. P. Strunk, Appl. Phys. Lett. **82**, 4471 (2003).
[2] D. Cherns, W.T. Young, and F.A. Ponce, Mater. Sci. Eng. B **50**, 76 (1997).
[3] D. Cherns, W.T. Young, J.W. Steeds, F.A. Ponce, and S. Nakamura, J. Cryst. Growth **178**, 201 (1997).
[4] F. Gloux, P. Ruterana, and G. Nouet, Phys. Status Solidi C **3**, 1815 (2006).
[5] E. Valcheva, T. Paskova, P. O. Å. Persson, and B. Monemar, Phys. Status Solidi A **194**, 532 (2002).
[6] E. Valcheva, T. Paskova, and B. Monemar, J. Cryst. Growth **255**, 19 (2003).
[7] T.B. Wei, R.F. Duan, J.X. Wang, J.M. Li, Z.Q. Huo, and Y.P. Zeng, Microelectr. J. **39**, 1556 (2008).
[8] L. Liu and J.H. Edgar, Mater. Sci. Eng. R **37**, 61 (2002).
[9] D.D. Koleske, M.E. Coltrin, K.C. Cross, C.C. Mitchell, and A.A. Allerman, J. Cryst. Growth **273**, 86 (2004).
[10] D.D. Koleske, M.E. Coltrin, and M.J. Russell, J. Cryst. Growth **279**, 37 (2005).
[11] J. Prazmowska, R. Korbutowicz, R. Paszkiewicz, A. Szyszka, J. Serafinczuk, A. Podhorodecki, J. Misiewicz, and M. Tlaczala, Vacuum **82**, 988 (2008).
[12] R. Cadoret, J. Cryst. Growth **205** 123 (1999).
[13] H. Ashraf, J.L. Weyher, G.W.G. van Dreumel, A. Gzregorzyck, and P.R. Hageman, J. Cryst. Growth **310**, 3957 (2008).
[14] F. Scholz, P. Brückner, F. Habel, M. Peter, and K. Köhler, Appl. Phys. Lett. **87**, 181902 (2005).
[15] J.L. Weyher, S. Lazar, L. Macht, Z. Liliental-Weber, R.J. Molnar, S.Muller, V.G.M. Sivel, G. Nowak, and I. Grzegory, J. Cryst. Growth **305**, 384 (2007).
[16] R. Lewandowska, J.L. Weyher, J.J. Kelly, L. Konczewicz, and B. Lucznik, J. Cryst. Growth **307**, 298 (2007).
[17] P. Gay, P.B. Hirsch, and A. Kelly, Acta Met. **1**, 315 (1953).
[18] M.J. Hordon and B.L. Averbach, Acta Metall. **9**, 237 (1961).
[19] J.L. Weyher, R. Lewandowska, L. Macht, B. Lucznik, and I. Grzegory, Mater. Sci. Semicond. Process. **9**, 175 (2006).
[20] C.R. Kim, J.Y. Lee, C.M. Shin, J.Y. Leem, H. Ryu, J.H. Chang, H.C. Lee, C.S. Son, W.J. Lee, W.G. Jung, S.T. Tan, J.L. Zhao, and X.W. Sun, Solid State Commun. **148**, 395 (2008).
[21] F.C. Frank, Adv. Phys. **1**, 91 (1952).
[22] L. Zhao, T. Yu, J. Wu, T. Daia, Z. Yanga, and G. Zhanga Appl. Surf. Sci., article in press, doi:10.1016/j.apsusc.2009.09.082
[23] C.E.C. Dam, P.R. Hageman, W.J.P. van Enckevort, T. Bohnen, and P.K. Larsen, J. Cryst. Growth **307**, 19 (2007).